RSC Advances

PAPER

View Article Online
View Journal | View Issue

Cite this: *RSC Adv.*, 2016, **6**, 39159

MoS_2 ultrathin nanoflakes for high performance supercapacitors: room temperature chemical bath deposition (CBD)

Swapnil S. Karade,[a] Deepak P. Dubal[b] and Babasaheb R. Sankapal*[a]

Received 18th February 2016
Accepted 7th April 2016

DOI: 10.1039/c6ra04441g

www.rsc.org/advances

Homogeneous ultrathin nanoflakes of MoS_2 thin films have been successfully developed by simple and low cost room temperature chemical bath deposition (CBD) method which further applied as electrode material for high-performance supercapacitors. The surface morphological analysis revealed uniform growth of MoS_2 nanoflakes on whole substrate surface. Structural analysis confirms the formation of rhombohedral crystal structure of MoS_2. The electrochemical performances were tested by cyclic voltammetry, galvanostatic charge/discharge and electrochemical impedance techniques. Different electrolytes were tested in order to find suitable electrolyte for MoS_2 thin films. In addition, the effect of electrolyte concentrations on supercapacitive properties of MoS_2 thin film was investigated. Thus, MoS_2 ultrathin nanoflakes electrode exhibits excellent electrochemical performances with maximum specific capacitance of 576 F g^{-1} at 5 mV s^{-1} and good cycling stability of 82% over 3000 cycles.

Introduction

In recent years, supercapacitors have become a new research hot spot in the field of energy storage due to their high levels of electrical power, large specific energy, fast charging–discharging rates and environmental protection.[1,2] As rechargeable power sources, supercapacitors also known as electrical double layer capacitor (EDLC) with excellent power and energy densities, have gathered increasing attention for applications that demand high operating power levels, such as consumer electronics, memory back-up systems, industrial power, energy management, public transportation, and military devices.[3,4] In this regard, different batteries and high performance capacitors are the focus of the scientific community.[5] According to the charge storage mechanisms, supercapacitors can be divided into two types. One is pseudocapacitor which is a surface redox reaction, usually includes transition metal oxides or hydroxides, conducting polymers, poly-oxometalates as electrode materials.[6,7] The other is electric double layer capacitors (EDLCs) which is based on charge separation at the electrode/electrolyte interface, mainly carbon based materials such as carbon nanospheres, carbon nanotubes and graphene.[8,9]

Recently, pseudo-capacitive nanomaterials (metal oxides and conducting polymers) and carbon nanotubes nanocomposites materials have attracted great attention based on the combination of the excellent properties of both the individual materials and their synergistic effects for electrode materials.[10–15] Among the electrode materials, metal sulfides are also known to be electrochemically active materials for supercapacitor applications, but to date very few metal sulfides, such as WS_2, MoS_2, CoS, NiS, SnS and ZnS, have been employed to fabricate supercapacitor electrodes due to their high conductivities.[2,16–22] Among the metal sulfides, molybdenum disulfide (MoS_2) has a layered structure like graphite with strong interlayer covalent bonds separated by weak van der Waals forces.[23,24] Due to its high surface area, electrical conductivity and sheet-like morphology, it can exhibit better capacitive properties. As compared to metal oxides and graphite, MoS_2 could be better electrode for supercapacitor applications because of its higher intrinsic fast ionic conductivity than oxides and higher theoretical capacity than graphite.[25–27] Many of the metal oxides as well as carbon materials having ultrathin nanostructures have been used for supercapacitor application.[28–30]

A very few reports on MoS_2 are available for supercapacitors application. Krishnamoorthy *et al.*[16] reported sphere like nanostructures with capacitance of 106 F g^{-1} at the scan rate of 5 mV s^{-1}. Also Ilanchezhiyan *et al.*[17] reported spherically clustered MoS_2 nanostructures for electrode applications with the maximum specific capacitance of 122 F g^{-1}. Ramadoss *et al.*[18] studied the electrochemical behavior of hydrothermally synthesized mesoporous MoS_2 nanostructure in KCl and Na_2SO_4 electrolyte. Apart from this, many of the researchers

[a]*Nanomaterials and Device Laboratory, Department of Applied Physics, Visvesvaraya National Institute of Technology, South Ambazari Road, Nagpur, 440010 Maharashtra, India. E-mail: brsankapal@gmail.com; Fax: +91 712 2223230; Tel: +91 712 2801170*

[b]*Catalan Institute of Nanoscience and Nanotechnology (ICN2), The Barcelona Institute of Science and Technology (CSIC-BIST), Campus UAB, Bellaterra, 08193 Barcelona, Spain*

have been reported the composite of C/MoS_2, MoS_2–graphene, 2D MoS_2 on reduced graphene oxide, MoS_2–multiwalled carbon nanotubes with the excellent supercapacitor properties.[25,31–33] However, present investigation reports very simple chemical bath deposition (CBD) method for synthesis of MoS_2 nanoflakes for supercapacitor application, which is not reported as per our knowledge. This CBD method is very simple, inexpensive and can be used for large area deposition.

In this paper, we report synthesis of MoS_2 ultrathin nanoflakes by CBD at room temperature directly on stainless steel substrate which are further used as electrode material for supercapacitor. The electrochemical performances of as deposited MoS_2 thin film were studied in different electrolytes and different electrolyte concentrations through cyclic voltammetry, charge–discharge studies, and electrochemical impedance measurements. The electrochemical properties suggest that, MoS_2 nanoflakes electrode exhibits excellent specific capacitance of 576 F g^{-1} at 5 mV s^{-1} with good cycling stability of 82% over 3000 cycles.

Materials and method

Materials used

Ammonium molybdate (LOBA chemie), sulfuric acid extra pure 98% (LOBA chemie) and sodium sulfide flakes purified (Merck), stainless steel substrate (305 grade) have been used.

Preparation of MoS_2 thin film

MoS_2 thin films were deposited by chemical bath deposition method (CBD) at room temperature (RT, 300 K). Briefly, 10 ml aqueous solution of 1 mM ammonium molybdate ($(NH_4)_6Mo_7O_{24}$) was used as a source of molybdenum in 50 ml beaker. Then, 0.5 ml of 1 M sulphuric acid (H_2SO_4) was added into the above solution to make it acidic. Later, 10 ml aqueous solution of 0.2 M sodium sulfide (Na_2S) was added into above bath as sulphur source. The colour of solution changes to light brown. Well cleaned stainless steel substrates were vertically immersed in the bath at room temperature with constant stirring. After some time, precipitation was started in the solution. During precipitation, a heterogeneous reaction occurred and the brown coloured MoS_2 thin film was deposited on the substrates. Stainless steel substrate coated with MoS_2 thin film was taken out after 1 h from the bath, washed with double-distilled water, dried in air and stored in an airtight container. The schematic representation of MoS_2 nanoflakes is shown in Fig. 1.

Material characterization

Structural arrangement of molybdenum sulfide (MoS_2) films was carried out with an X-ray diffractometer (XRD) using Cu-Kα radiation ($\lambda = 1.54$ Å) (System Ultima IV of Rigaku Corporation, Japan). Chemical bonding were studied with Fourier transform infrared (FTIR) spectra recorded on a JASCO 410 model. X-ray photoelectron spectroscopy (XPS) was done by Electron Spectra on for Chemical Analyzer (ESCA) VG Multilab2000, Thermo VG Scientific UK. The film surface morphology was observed by Field emission scanning electron micrograph (FESEM).

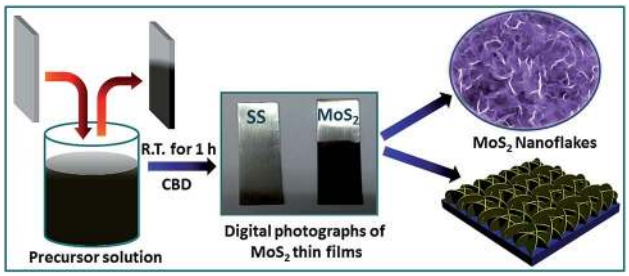

Fig. 1 Schematic representation for formation of MoS_2 nanoflakes.

Transmission electron microscopy (TEM) images were taken with a JEOL JEM-2100 operated at 200 kV. Supercapacitor formation and respective studies were carried out using the Potentiostat/Galvanostat PARSTAT 4000 (Princeton Applied Research, USA).

Electrochemical measurements were carried out using three electrode cell configurations with MoS_2 as the working electrode, platinum as the counter electrode and Ag/AgCl as the reference electrode with Na_2SO_4 as an electrolyte. The cyclic voltammetry measurements of the MoS_2 electrode were performed at different scan rates in a potential window of −0.1 to −0.8 V. The charge–discharge characterization was performed at different specific current within a potential window of −0.1 to −0.8 V. Electrochemical impedance measurements were carried out between 0.01 Hz and 100 MHz with AC amplitude of 10 mV.

Result and discussion

Film formation and reaction mechanism

The thin films formation by chemical bath deposition (CBD) method is based on the principle of controlled precipitation.[34] Film growth dominates in two different ways: (i) *via* ion-by-ion condensation of materials and (ii) by the adsorption of colloidal particles from the solution on the substrate. At the initial stage H_2SO_4 reacts with $(NH_4)_6Mo_7O_{24}$ under room temperature chemical bath deposition and formation of $(NH_4)_2MoO_4$ takes place as

$$(NH_4)_6Mo_7O_{24} + 4H_2SO_4 \rightarrow 7(NH_4)_2MoO_4 + 4(NH_4)_2SO_4 + 4H_2O \quad (1)$$

At the second stage, Na_2S decomposed into H_2S with distilled water as

$$Na_2S + 2H_2O \rightarrow 2NaOH + H_2S \quad (2)$$

The produced H_2S reacts with $(NH_4)_2MoO_4$ under acidic condition and brown colored MoS_2 is formed as

$$4(NH_4)_2MoO_4 + 3H_2SO_4 + 9H_2S \rightarrow 4MoS_2 + 4(NH_4)_2SO_4 + 12H_2O \quad (3)$$

Structural studies

XRD pattern of the MoS_2 nanoflakes thin film on stainless steel substrate is shown in Fig. 2(a). As projected in Fig. 2(a), the peak

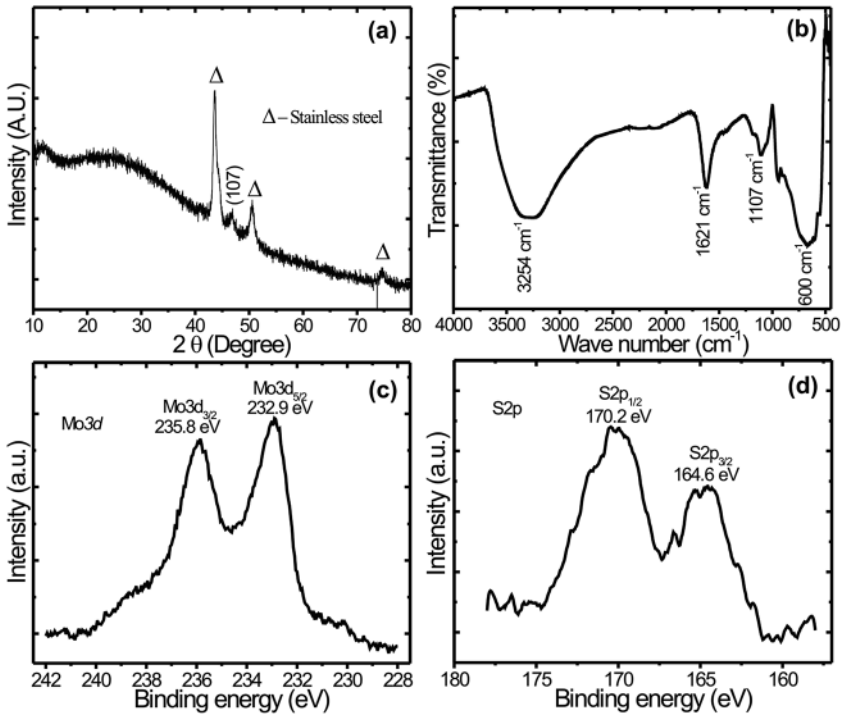

Fig. 2 (a) XRD pattern of MoS_2 (b) FTIR spectra of MoS_2 sample. (c and d) Core level XPS spectrums of MoS_2 film for Mo 3d and S 2p.

at 47.8° corresponds to the (107) plane, indexed to the rhombohedral structure of MoS_2 (JCPDS card no. 77-0341). The broad and low intensity peak indicates the formation of nanocrystalline MoS_2. The nanocrystalline nature of MoS_2 is beneficial for supercapacitor application, as it allows easy and fast access for intercalation/deintercalation of electrolyte ion in the active electrode material.[35] The peaks marked by triangle are associated to the stainless steel substrate.

The FT-IR measurement was carried out in order to obtain the bending and stretching vibrations of functional group present in the samples. As shown in Fig. 2(b), FTIR spectrum of MoS_2, the peaks observed at about 600 cm^{-1} are assigned to Mo–S vibration.[33] The peak corresponding to 1106 cm^{-1} is may be S–O (sulfide oxide) asymmetric stretching. Moreover, a broad absorption band at about 3254 cm^{-1} and 1621 cm^{-1} appear in the FTIR spectra are assigned to stretching vibrations of the O–H bonds which can be assigned to intercalated water.[36]

The XPS was used to find the composition of the as-prepared MoS_2 film. Fig. 2(c and d) are the survey scan of MoS_2 thin film which exhibits characteristic peaks of Mo 3d and S 2p with their corresponding binding energies. Fig. 2(c) Mo 3d spectrum shows two strong peaks sited at 232.9 and 235.8 eV, which are attributed to the doublet of Mo $3d_{5/2}$ and Mo $3d_{3/2}$ spin orbitals, respectively, and confirmed the formation of MoS_2.[32] Similarly, Fig. 2(d) S 2p spectrum exhibited peaks at 164.6 and 170.2 eV, which correspond to the S $2p_{3/2}$ and S $2p_{1/2}$ orbitals of the divalent sulfide ions (S^{2-}) respectively.[37]

Surface morphological study

For electrochemical supercapacitor application, the surface morphology of an active electrode material has a great importance, as the electrochemical reactions occur at or near the surface of electrode. Fig. 3(a and b) demonstrates the surface morphology of MoS_2 thin film at two different magnifications. The surface of chemically deposited MoS_2 thin film reveals that formation of nanoflakes. The nanoflakes morphology is advantageous for efficient ion/electron transport and for better accommodating the volume variation.[38] The compositions of the chemically prepared MoS_2 samples on stainless steel substrate were analysed by energy dispersive X-ray analysis (EDAX). Fig. 3(c) shows the EDAX image of the MoS_2 nanoflakes. EDAX analysis confirmed that the MoS_2 nanoflakes structure is composed of Mo and S. The energy of Mo and S elements are obtained within the range of 2 to 2.6 keV which is similar to previously reported mesoporous MoS_2 nanostructure.[18] The all other peaks obtained in EDAX pattern are the contribution of stainless steel substrate.

TEM images of MoS_2 sample is shown in Fig. 3(d). The TEM analysis clearly indicates the formation of clusters of ultrathin nanoflakes, interconnected and with sizes in the range 2–3 nm; these are in good agreement with the results from the SEM images. Such ultrathin nanoflakes provided easy access for electrolyte ions, which is very useful for supercapacitors. The corresponding SAED pattern Fig. 3(e) shows diffuse rings, indicating that the flakes are polycrystalline.

Electrochemical studies

The capacitive performances of the MoS_2 thin film electrodes were evaluated by cyclic voltammetry (CV). In order to find suitable electrolyte for better electrochemical behavior, the CV curves of MoS_2 thin film were recorded in 0.5 M Na_2SO_3, KCl, K_2SO_4, NaOH, KOH, Na_2S, Na_2SO_4 electrolytes at scan rate of

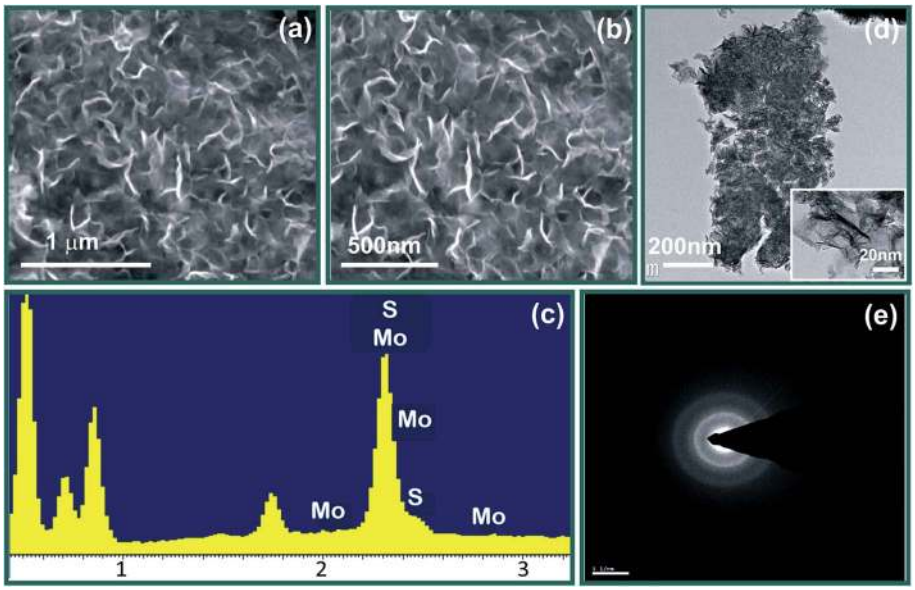

Fig. 3 (a and b) FE-SEM images of MoS_2 (c) EDAX pattern of MoS_2 (d) TEM image of MoS_2 sample (e) shows SAED pattern of MoS_2.

100 mV s^{-1} (see Fig. 4(a)). It can be observed that some of the curves exhibit an almost rectangular and symmetric shape which indicates non-faradaic charging (electrochemical double layer capacitance). In Fig. 4(a), MoS_2 thin film electrode is showing redox behavior in the NaOH and KOH electrolytes which may be attributed to the redox reactions between strong basic electrolytes and MoS_2.

There are two possible predicted mechanisms. The first one is non-faradaic process might be due to the formation of a double layer at the electrode/electrolyte interface during the adsorption of protons or cations on the MoS_2 thin film.

$$(MoS_2)_{surface} + C^+ (Na^+ \text{ or } K^+) + e^- \leftrightarrow (MoS_2 - C^+)_{surface} \quad (4)$$

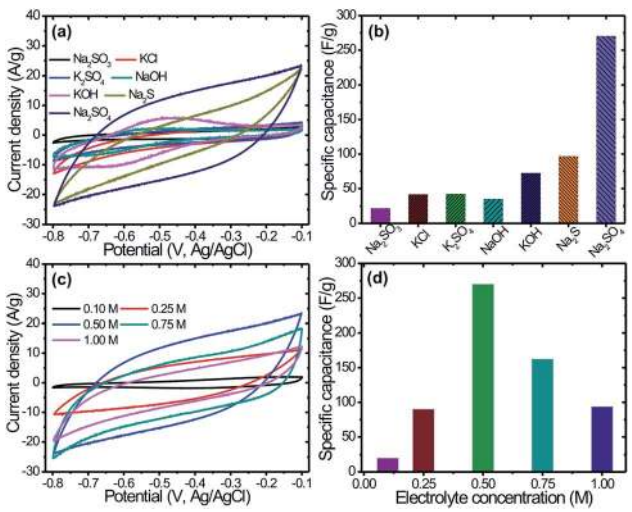

Fig. 4 (a) CV curves of MoS_2 at different electrolytes (b) variation of specific capacitance with electrolytes (c) effect of Na_2SO_4 electrolyte concentrations on CV curves at 100 mV s^{-1} scan rate (d) variation of specific capacitance with different concentrations of Na_2SO_4.

The second is based on the pseudocapacitive behavior due to the faradaic charge transfer process. During the redox process ions such as protons (H^+) and/or alkali metal cations (Na^+ and K^+) may diffuse into the interlayer of MoS_2 structure.

$$MoS_2 + C^+ + e^- \leftrightarrow MoS - SC^+ \quad (5)$$

The values of specific capacitance of the as prepared electrode was calculated from CV curves using a following equation

$$C_s = \frac{\int_{V_i}^{V_f} I(V)\mathrm{d}V}{m\nu(V_f - V_i)} \quad (6)$$

where, C_s is specific capacitance (F g^{-1}), ν is potential scan rate (mV s^{-1}), $(V_f - V_i)$ is operational potential window, I is the current response (mA) of the MoS_2 electrode for unit area (1 cm^2) dipped in electrolyte and m is deposited mass of MoS_2 on 1 cm^2 surface of stainless steel substrate. The mass deposited of MoS_2 was 0.58 mg cm^{-1} taken by sensitive microbalance. Fig. 4(b) shows that variation of specific capacitance of MoS_2 thin film with electrolytes at 100 mV s^{-1} scan rate. It is seen that, maximum specific capacitance of MoS_2 electrode was 270 F g^{-1} observed in 0.5 M Na_2SO_4 electrolyte.

If it is going to be a contribution from the double layer, where the charge is stored mainly in the electrolyte, the change in the electrolyte concentration will have a direct effect on the capacitance value.[39] In order to check the suitable electrolyte concentration for better capacitive properties, the concentration of electrolyte was changed from 0.1 to 1 M (Fig. 4(c)). The effect of concentration of Na_2SO_4 electrolyte was studied by keeping the scan rate and potential window constant (100 mV s^{-1} and −0.1 to −0.8 V). In the present case, the current under the curve increases as the Na_2SO_4 concentration is increased from 0.1 M to 0.5 M; thereafter further increase in concentration peel off of the sample was observed. Fig. 4(d) shows the

variation of specific capacitance with different electrolyte concentrations. It is seen that, the maximum specific capacitance of MoS_2 electrode was 270 F g^{-1} observed at 0.5 M Na_2SO_4 electrolyte concentration. If the electrolyte concentration is high, the ion transport within the electrode layer will be easier, leading to an effective building-up for double layer. However, if the electrolyte concentration is further increased, the ion activity may be reduced due to less water hydration, resulting in decreases ion mobility.[40] Therefore, all further electrochemical performances were carried out in 0.5 M Na_2SO_4 electrolyte.

The capacitive performances of the MoS_2 electrodes were evaluated at different scan rate (Fig. 5(a)) in 0.5 M Na_2SO_4. It is seen, that all the curves exhibit almost rectangular and symmetric shapes which indicates non-faradaic charging *i.e.* electrochemical double layer capacitance. In addition, the CV curve area increases with increasing scan rate from 1 to 200 mV s^{-1}, which reveals the capacitive behavior of the electrodes. Further, the shape of the CV curves does not change evidently even at higher scan rates and the total current increases with increasing potential scan rates, which demonstrates a good rate property and excellent capacitive behavior for the MoS_2 thin films electrode. In addition, it can be seen that the broadening of CV curves shifts in the positive direction with increase in the scan rates, which might be due to the internal resistance of the electrode. Fig. 5(b) shows the variation of specific capacitance with scan rates. Note that MoS_2 nanoflakes exhibited a maximum specific capacitance of 576 F g^{-1} at a scan rate of 5 mV s^{-1}. Moreover, a decrease in capacitance with increased scan rate is observed, which due to charge resistive behavior of the electrode material at higher scan rate. Several authors have investigated supercapacitive properties of MoS_2 thin films. For example, Ilanchezhiyan *et al.*[17] reported the value of specific capacitance 122 F g^{-1} at 5 mV s^{-1} scan rate in 1 M Na_2SO_4 electrolyte for spherically clustered MoS_2 nanostructures synthesized by hydrothermal route, and Ramadoss *et al.*[18] reported the value of specific capacitance 403 F g^{-1} at 1 mV s^{-1} scan rate in KCl electrolyte for mesoporous MoS_2 nanostructure synthesized by the hydrothermal route. The reason for high specific capacitance in the present investigation might be unique, as the nanoflakes like architecture provided a less resistive behaviour at lower scan rate. However, the previously reported specific capacitances values are tabulated in Table 1 in comparison with present one.[16–18,41,42]

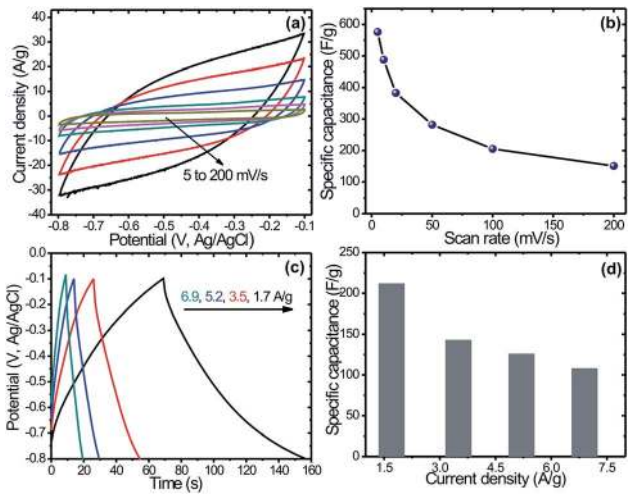

Fig. 5 (a) CV curves of MoS_2 electrode at different scan rates in 0.5 M Na_2SO_4 (b) specific capacitances of the MoS_2 electrode at different scan rates from 1 to 200 mV s^{-1} (c) galvanostatic charge–discharge curves of the MoS_2 electrode at different specific currents in 0.5 M Na_2SO_4 (d) specific capacitance of MoS_2 electrode at different specific currents.

Fig. 5(c) shows the galvanostatic charge–discharge (GCD) curves of MoS_2 electrode measured at different specific currents (1.7, 3.5, 5.2 and 6.9 A g^{-1}) in 0.5 M Na_2SO_4 electrolyte. It is seen that, all the curves exhibit almost symmetric and triangular shapes, indicating the capacitive behavior of the electrodes.

Table 1 The comparative chart of MoS_2 electrode for supercapacitor application

Material	Method	Morphology	Specific capacitance (F g^{-1})	Retention	Ref.
MoS_2	Hydrothermal	Sphere like	106 at 5 mV s^{-1} in 1 M Na_2SO_4	—	16
MoS_2	Hydrothermal route	Nanosphere	122 at 0.5 A g^{-1} in 1 M Na_2SO_4	—	17
MoS_2	Hydrothermal route	Mesoporous	376 and 403 at 1 mV s^{-1} in 1 M Na_2SO_4 and 1 M KCl	80% 2000 cycles	18
MoS_2	Two step hydrothermal	3D flower like	168 at 1 A g^{-1} in 1 M KCl	92.6% 3000 cycles	41
MoS_2	CBD	Ultrathin nanoflakes	576 at 5 mV s^{-1} in 0.5 M Na_2SO_4	82.2% 3000 cycles	This work
MoS_2	Hydrothermal	Flower like	129.2 F g^{-1} at 1 A g^{-1} in 1 M Na_2SO_4	85.1% 500 cycles	42
MoS_2	CVD	Nanowall	100 F g^{-1} at 1 mV s^{-1} in 0.5 M H_2SO_4	—	39

Table 2 Electrochemical supercapacitive performances of MoS_2 electrode

Specific current (A g^{-1})	Discharge time (s)	Specific capacitance (F g^{-1})	Energy density (W h kg^{-1})	Power density (kW kg^{-1})
1.7	87	214.28	14.58	0.603
3.5	29	142.86	9.72	1.207
5.2	16	118.23	8.05	1.810
6.9	11	108.37	7.37	2.414

Initial voltage drop during discharge was attributed to internal resistance of the MoS_2 material. Note that the initial voltage loss was small even at the high current densities, indicating fast CV response and low internal resistance in the supercapacitors. The specific capacitance (C_s) can also be calculated from the galvanostatic charge–discharge curves using a familiar equation.

$$C_s = \frac{I \times \Delta t}{m \times \Delta V} \quad (7)$$

where, I is the discharge current (A), Δt is the discharge time (s), m is the mass of the active material (g) and ΔV is the potential window (V). The specific capacitances calculated are found to be 214, 142, 118 and 108 F g^{-1} in 0.5 M Na_2SO_4 solution, obtained at current densities of 1.7, 3.5, 5.2 and 6.9 A g^{-1}, respectively (Fig. 5(d)). The obtained result implies that, the relatively good specific capacitance retention ratio of the electrode at current densities ranging from 1.7 to 6.9 A g^{-1}.

Energy density (ED) and power density (PD) are the most important parameters of an electrochemical supercapacitor device which determine its operational efficiency and performance. The ED and PD values of MoS_2 nanoflakes are derived from the GCD curves at different specific currents according to the following equations:

$$E = \frac{0.5 \times C_s \times \Delta V^2}{3.6} \quad (8)$$

$$P = \frac{E \times 3600}{\Delta t} \quad (9)$$

where, C_s is specific capacitance, Δt is discharging time, ΔV is the potential during charging and discharging cycles. The specific capacitance, ED and PD values at different specific currents are evaluated in Table 2 and are plotted in Ragone plot (Fig. 6(a)). It is seen that, MoS_2 electrode provides good energy density as compared to the conventional capacitor and higher power density than the batteries, which is requisite as a supercapacitor.

In order to understand the fundamental behavior of the supercapacitor electrode, electrochemical impedance spectroscopy (EIS) studies has been performed at a frequency range of 0.01 Hz to 100 kHz in 0.5 M solution of Na_2SO_4. The EIS data was analysed using Nyquist plots, which show the frequency response of the electrode/electrolyte system and plotted as the imaginary component (Z'') of the impedance against the real component (Z'). Fig. 6(b) represents the EIS spectra with the equivalent circuit of MoS_2 electrodes which show one partially undercrossed and low semicircle at the high frequency region and straight lines at low frequency region.[43] The observation of very small equivalent series resistance (R_s) is about 8.50 Ω at the intercept on real axis and diameter of the arc in the high frequency range is likely attributed to the charge transfer resistance (R_{ct}) and is about 1.75 Ω. The presence of a straight line nearly parallel to the imaginary axis revealed the ideal capacitive behavior of the MoS_2 electrode.

Long term cyclic stability is one of the important criterions for the practical applications of supercapacitor devices. Fig. 6(c) shows the cyclic tests of the MoS_2 electrodes for 3000 cycles at the scan rate of 100 mV s^{-1} measured using CV technique. It clearly shows that the MoS_2 material possesses capacitance retention of about 82.25% even after 3000 cycles. The enhanced electrochemical performance of the MoS_2 electrode is mainly due to its nanoflakes morphology, which provided the large surface area, and an efficient ion and electron transport. This study suggested the long term cyclic stability of MoS_2 for supercapacitor applications.

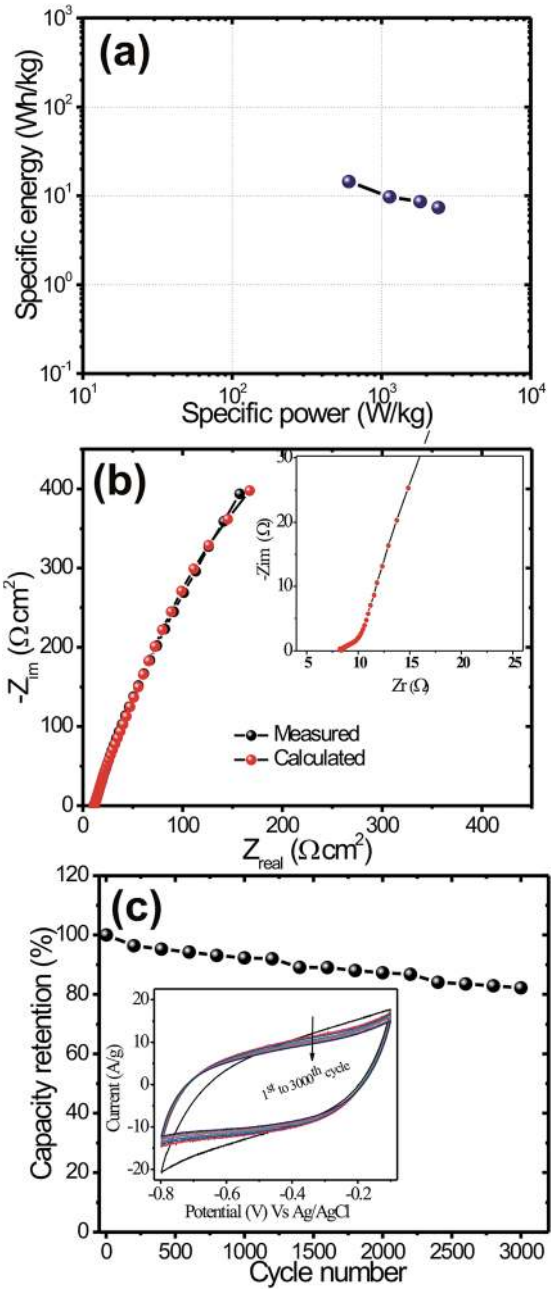

Fig. 6 (a) Ragone plot of MoS_2 electrode (b) Nyquist plots for the MoS_2 electrode with an equivalent circuit (c) retention stability of MoS_2 electrode for 3000 cycles at 100 mV s^{-1} scan rate.

Conclusions

We have successfully grown nanoflakes like MoS_2 architecture by simple, cost effective and room temperature CBD method. The physico-chemical characterizations have shown the formation of rhombohedral, 3D-nanoflakes like MoS_2 thin films. This unique nanostructured MoS_2 exhibited high specific capacitance of about 576 F g^{-1} at 5 mV s^{-1} scan rate. Furthermore, high energy density of 14.58 W h kg^{-1} as well as good long term cycling stability of 82% over 3000 cycles. Thus these encouraging results suggest that the MoS_2 nanoflakes can serve as promising electrode materials for high performance supercapacitors.

Acknowledgements

BRS and SSK would like to thank the SERB project, Govt. of India (Do. No. SB/S2/CMP/032/2013; 04/06/2013).

References

1 H. Pang, S. Wang, W. Shao, S. Zhao, B. Yan, X. Li, S. Li, J. Chen and W. Ou, *Nanoscale*, 2013, **5**, 5752–5757.
2 S. Ratha and C. S. Raut, *ACS Appl. Mater. Interfaces*, 2013, **5**, 11427–11433.
3 B. E. Conway, *Electrochemical supercapacitor, scientific fundamentals and Technological applications*, Kluwer Academic/Plenum press, New York, 1999.
4 C. Liu, F. Li, L. P. Ma and H. M. Cheng, *Adv. Mater.*, 2010, **22**, E28–E62.
5 D. P. Dubal, O. Ayyad, V. Ruiz and P. Gomez-Romero, *Chem. Soc. Rev.*, 2015, **44**, 1777–1790.
6 D. P. Dubal, J. Suarez-Guevara, D. Tonti, E. Enciso and P. Gomez-Romero, *J. Mater. Chem. A*, 2015, **3**, 23483–23492.
7 G. Ma, H. Peng, J. Mu, h. Huang, X. Zhau and Z. Lei, *J. Power Sources*, 2013, **229**, 72–78.
8 M. Chhowalla, H. S. Shin, G. Eda, L. J. Li, K. P. Loh and H. Zhang, *Nat. Chem.*, 2013, **5**, 263–275.
9 J. Feng, X. Sun, C. Wu, L. Peng, C. Lin, S. Hu, J. Yang and Y. Xie, *J. Am. Chem. Soc.*, 2011, **133**, 17832–17838.
10 D. P. Dubal, J. G. Kim, Y. Kim, R. Holze, C. D. Lokhande and W. B. Kim, *Energy Technol.*, 2014, **2**, 325–341.
11 H. Jiang, P. S. Lee and C. Li, *Energy Environ. Sci.*, 2013, **6**, 41–53.
12 H. Jiang, J. Ma and C. Li, *Adv. Mater.*, 2012, **24**, 4196–4201.
13 H. Jiang, Y. Dai, Y. Hu, W. Chen and C. Li, *ACS Sustainable Chem. Eng.*, 2014, **2**, 70–74.
14 Y. Yan, Q. Cheng, G. Wang and C. Li, *J. Power Sources*, 2011, **196**, 7835–7840.
15 Y. Yan, Q. Cheng, Z. Zhu, V. Pavlinek, P. Saha and C. Li, *J. Power Sources*, 2013, **240**, 544–550.
16 K. Krishnamoorthy, G. K. Veerasubramani, S. Radhakrishnan and S. J. Kim, *Mater. Res. Bull.*, 2014, **50**, 499–502.
17 P. Ilanchezhiyan, G. Mohankumar and T. W. Kang, *J. Alloys Compd.*, 2015, **634**, 104–108.
18 A. Ramadoss, T. Kim, G. S. Kim and S. J. Kim, *New J. Chem.*, 2014, **38**, 2379–2385.
19 L. Zhang, H. B. Wu and X. W. Lau, *Chem. Commun.*, 2012, **48**, 6912–6914.
20 J. Yang, X. Duan, Q. Qin and W. Zheng, *J. Mater. Chem. A*, 2013, **1**, 7880–7884.
21 M. Jayalakshmi, M. M. Rao and B. M. Choudhari, *Electrochem. Commun.*, 2004, **6**, 1119–1122.
22 M. Jayalakshmi and M. M. Rao, *J. Power Sources*, 2006, **157**, 624–629.
23 K. H. Hu, X. G. Hu, Y. F. Xu and J. D. Sun, *J. Mater. Sci.*, 2010, **45**, 2640–2648.
24 J. Zhao, Z. Zhang, S. Yang, H. Zheng and Y. Li, *J. Alloys Compd.*, 2013, **559**, 87–91.
25 K. J. Huang, L. Wang, Y. J. Liu, Y. m. Liu, H. B. Wang, T. Gan and L. L. Wang, *Int. J. Hydrogen Energy*, 2013, **38**, 14027–14034.
26 N. Zheng, X. Bu and P. Feng, *Nature*, 2003, **426**, 428–432.
27 J. Xiao, D. Choi, L. Cosimbescu, P. Koech, J. Liu and J. P. Lemmon, *Chem. Mater.*, 2010, **22**, 4522–4524.
28 Y. Dai, H. Jiang, Y. Hu, Y. Fu and C. Li, *Ind. Eng. Chem. Res.*, 2014, **53**, 3125–3130.
29 H. Jiang, C. Li, T. Sun and J. Ma, *Nanoscale*, 2012, **4**, 807–812.
30 Z. Zhu, Y. Hu, H. Jiang and C. Li, *J. Power Sources*, 2014, **246**, 402–408.
31 B. H. Hu, X. Qin, A. M. Asiri, K. A. Alarmy, A. O. Al-Youbi and X. Sun, *Electrochim. Acta*, 2013, **100**, 24–28.
32 E. G. S. Firmiano, A. C. Rabelo, C. J. Dalmaschio, A. N. Pinheiro, E. C. Pereira, W. H. Schreiner and E. R. Leite, *Adv. Energy Mater.*, 2014, **4**, 1301380–1301387.
33 K. J. Huang, L. Wang, J. Z. Zhang, L. L. Wang and Y. P. Mo, *Energy*, 2014, **67**, 234–240.
34 D. P. Dubal, G. S. Gund, R. Holze and C. D. Lokhande, *J. Power Sources*, 2013, **242**, 687–698.
35 N. R. Chodankar, D. P. Dubal, G. S. Gund and C. D. Lokhande, *Electrochim. Acta*, 2015, **165**, 338–347.
36 M. A. S. Ana, E. Benavente, P. G. Romero and G. González, *J. Mater. Chem.*, 2006, **16**, 3107–3113.
37 H. Lin, X. Chen, H. Li, M. Yang and Y. Qi, *Mater. Lett.*, 2010, **64**, 1748.
38 D. P. Dubal, P. Gomez-Romero, B. R. Sankapal and R. Holze, *Nano Energy*, 2015, **11**, 377–399.
39 J. M. Soon and K. P. Loh, *Electrochem. Solid-State Lett.*, 2007, **10**(11), A250–A254.
40 K. C. Tsay, L. Zhang and J. Zhang, *Electrochim. Acta*, 2012, **60**, 428–436.
41 X. Wang, J. Ding, S. Yao, X. Wu, Q. Feng, Z. Wang and B. Geng, *J. Mater. Chem. A*, 2014, **2**, 15958–15963.
42 K. J. Huang, J. Z. Zhang, G. W. Shi and Y. M. Liu, *Electrochim. Acta*, 2014, **132**, 397–403.
43 K. K. Purushothaman, M. Cuba and G. Muralidharan, *Mater. Res. Bull.*, 2012, **47**, 3348–3851.